IOPscience iopscience.iop.org

The origin of the weak ferroelectric-like hysteresis effect in paraelectric $Ba_{0.5}Sr_{0.5}TiO_3$ thin films grown epitaxially on $LaAlO_3$

This article has been downloaded from IOPscience. Please scroll down to see the full text article.

2006 J. Phys.: Condens. Matter 18 4709

(http://iopscience.iop.org/0953-8984/18/19/022)

View the table of contents for this issue, or go to the journal homepage for more

Download details:
IP Address: 129.252.86.83
The article was downloaded on 28/05/2010 at 10:41

Please note that terms and conditions apply.

INSTITUTE OF PHYSICS PUBLISHING JOURNAL OF PHYSICS: CONDENSED MATTER

J. Phys.: Condens. Matter **18** (2006) 4709–4718 doi:10.1088/0953-8984/18/19/022

The origin of the weak ferroelectric-like hysteresis effect in paraelectric $Ba_{0.5}Sr_{0.5}TiO_3$ thin films grown epitaxially on $LaAlO_3$

X H Zhu[1], L P Yong, H F Tian, W Peng, J Q Li and D N Zheng

Beijing National Laboratory for Condensed Matter Physics, Institute of Physics, Chinese Academy of Sciences, Beijing 100080, People's Republic of China

E-mail: xhzhu@ssc.iphy.ac.cn

Received 9 February 2006
Published 27 April 2006
Online at stacks.iop.org/JPhysCM/18/4709

Abstract

Perovskite $Ba_{0.5}Sr_{0.5}TiO_3$ (BST) thin films, with thickness of about 350 nm, have been epitaxially grown on (001) $LaAlO_3$ substrates by pulsed-laser deposition. The good crystallography and epitaxy characteristics were confirmed using x-ray diffraction and transmission electron microscopy (TEM). The dielectric properties of the BST thin films were measured with a planar capacitor configuration in the temperature range of 77–300 K. The capacitance–temperature characteristics, measured with no and several different DC biases, reveal that the BST films are in the paraelectric state at room temperature, with a very good dielectric tunability. However, a butterfly-shaped curve, typical for a ferroelectric material, was obtained from room temperature capacitance–voltage (C–V) measurements, suggesting a faint ferroelectric-like effect for the BST thin films. Careful dielectric property characterizations showed significant temperature and frequency dependence, probably indicating a behaviour of Maxwell–Wagner-type dielectric relaxation. As a result, the weak C–V hysteresis effect in our paraelectric BST thin films is believed to be ascribable both to oxygen vacancies and to the presence of other space charges, trapped at the grain boundaries and/or at the substrate/dielectric film interface, which give rise to local polar regions in the thin-film samples. Furthermore, this explanation is supported by cross-sectional TEM and off-axis electron holographic observations.

1. Introduction

Thin films of room temperature paraelectric barium strontium titanate ($Ba_{1-x}Sr_xTiO_3$, hereafter designated as BST) with $x > 0.35$ are of increasing technological interest because of their potential applications in electrically tunable microwave devices, such as frequency-agile filters,

[1] Author to whom any correspondence should be addressed.

© 2006 IOP Publishing Ltd Printed in the UK

voltage-controlled oscillators, phase shifters and antennas [1–4]. For these applications, a large electric field dependence of the nonlinear dielectric response, i.e., tunability, defined as $[\varepsilon(0) - \varepsilon(E_{\max})]/\varepsilon(0)$, and a low dielectric loss of the BST thin films are two prerequisites. Here, $\varepsilon(0)$ is the dielectric constant measured at zero applied bias and $\varepsilon(E_{\max})$ is the one measured at the maximum applied bias field. According to this principle, an appropriate Ba/Sr ratio should be adopted to make the Curie temperature (T_c) slightly lower than room temperature, which could ensure that the BST is in the paraelectric state and lead to the largest dielectric tunability, the highest dielectric constant and a relatively low loss tangent at room temperature. The ferroelectric phase must be avoided due to the fact that the ferroelectric polarization reversal and fatigue effect would drastically degrade the performance of the devices. However, grain boundaries, charged defects, mechanical stresses, interfaces and other microstructural details generally induce ferroelectric-like behaviours in paraelectric thin films, even in thin-film incipient ferroelectric systems such as $SrTiO_3$ [5–12]. One reason for this phenomenon was proposed by Pontes *et al*: an interfacial space charge effect [5, 7]. Another possible explanation was association with the presence of nanometre-sized polar regions in the thin-film samples due to oxygen vacancies and inhomogeneous strain from grain boundaries [8–11]. Until now, however, there have been few systematical results reported in the literature relating to this issue; hence to clarify its nature is not only of theoretical importance, but also of great technological significance for pushing this kind of thin-film material further for practical applications.

In this paper, we report the epitaxial growth of $Ba_{0.5}Sr_{0.5}TiO_3$ thin films on $LaAlO_3$ (LAO) substrates by pulsed-laser deposition, as well as their structural and dielectric property characterizations. In the case of the samples investigated here, a weak capacitance–voltage (C–V) hysteresis effect is confirmed to exist in the paraelectric BST thin films. The origin of the ferroelectric-like responses is presented and systematically discussed by combining careful dielectric property measurements with direct transmission electron microscopy (TEM) and off-axis electron holography observations.

2. Experimental details

The BST thin films were epitaxially grown on (001) LAO single-crystal substrates by pulsed-laser deposition using a KrF (248 nm wavelength) excimer laser system (Lambda Physik LPX 300cc) with a repetition rate of 5 Hz and 25 ns pulse duration. The pulsed-laser beam was focused by a quartz lens to a fluence of approximately 2 J cm^{-2} and directed at an angle of 45° onto the target. The target, a stoichiometric $Ba_{0.5}Sr_{0.5}TiO_3$ ceramic disc, was rotated during the ablation process to reduce nonuniform erosion. The substrate was placed parallel to the target at a distance of 55 mm. The BST film was deposited for 20 min at a substrate temperature of 800 °C in oxygen pressure of 25 Pa to a thickness of about 350 nm, which was checked by cross-sectional TEM measurements. After deposition, 1 atm high purity oxygen was introduced into the growth chamber; the as-deposited film was annealed at 600 °C for 30 min and then slowly cooled to room temperature.

The crystallographic structures of the BST thin films were analysed by means of x-ray diffraction (XRD) using characteristic Cu Kα x-rays. The microstructure and the interfacial space charge information observations were carried out by TEM and off-axis electron holography, respectively, utilizing a Philips CM200/FEG transmission electron microscope equipped with an electrostatic biprism. Detailed descriptions of the principle and instrumental parameters were reported elsewhere [13].

For dielectric property measurements of the dielectric constant and loss tangent characteristics, the interdigital capacitor technique was used. Firstly, about 100 nm thick Au

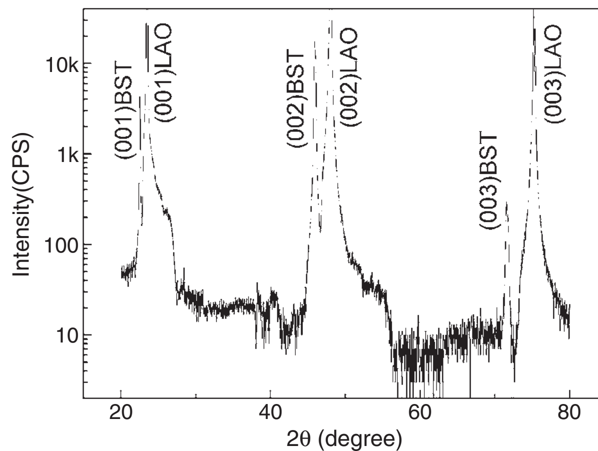

Figure 1. Typical θ–2θ XRD scans of the BST thin film grown on LAO. The film is grown in a pure single-orientation perovskite phase.

thin film was deposited by DC magnetron sputtering. Then, the Au film was etched into the required interdigital electrodes by photolithography. The capacitor consisted of 50 fingers that were 1 mm long, 10 μm wide and spaced 10 μm apart. The measurements were performed with an Agilent 4294A Precision Impedance Analyzer. The relative dielectric constant (ε_r) was extracted from the capacitance by using the conformal mapping results of Gevorgian *et al* [14, 15].

3. Results and discussion

The crystalline structure of the BST thin film, analysed by means of XRD θ–2θ scans, is shown in figure 1. Only $(00l)$ peaks of BST are observed, indicating that the films have been successfully grown in pure single-orientation perovskite phases. The crystallographic indices of both LAO and BST are referred to their cubic unit cells. The lattice constant (a_f) of the BST film is calculated to be 3.951 Å, only slightly larger than the 3.947 Å of the bulk counterpart due probably to oxygen vacancies in the as-grown thin films, which are common defects in oxide thin films. Similarly, the lattice constant (a_s) of the LAO substrate is found to be 3.790 Å. In consequence, a lattice mismatch ($(a_f - a_s)/a_s \times 100\%$) of about 4.2% between the BST film and the LAO substrate can be obtained. Because of such a large lattice mismatch, misfit dislocations are generated at the film/substrate interface during the BST film growth to relieve the in-plane compressive strain. This concept will be further confirmed in the following TEM observations.

The good structural properties of the BST thin films could also be confirmed by cross-sectional TEM observations. Figures 2(a) and (b) show a high resolution TEM (HRTEM) image and the corresponding selected-area electron diffraction (SAED) pattern, obtained at an interface area between the BST thin film and the LAO substrate. It is pointed out that no Fourier transformation was performed for figure 2(a). As can be seen in figure 2(a), the interface is very clean and sharp, without any trace of an interfacial reaction layer. Figure 2(b), a clear spot pattern, illustrates the well-defined epitaxial relationship between the film and substrate. Two sets of electron diffraction spots, arising, respectively, from the LAO substrate and the BST film, can be distinctly indexed, on the basis of the $LaAlO_3$ structure (a cubic unit cell with

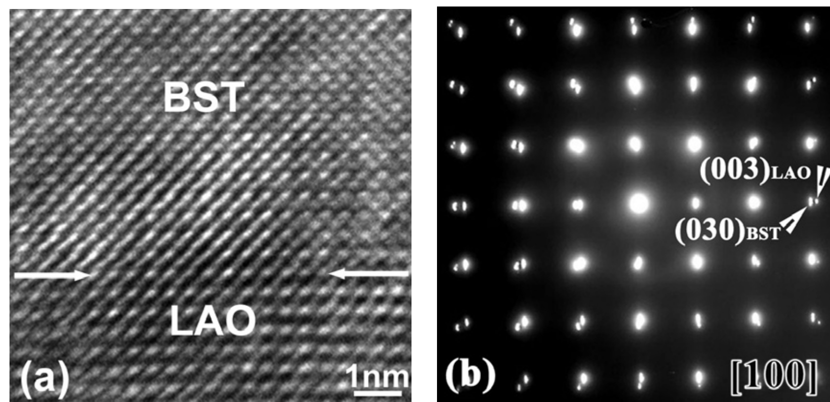

Figure 2. (a) Cross-sectional HRTEM image of the BST thin film on the LAO substrate and (b) corresponding SAED pattern, obtained at the interface between BST and LAO. Note that the quite clean and sharp interface, as well as the clear spot pattern, demonstrate the good quality of the thin film epitaxial growth.

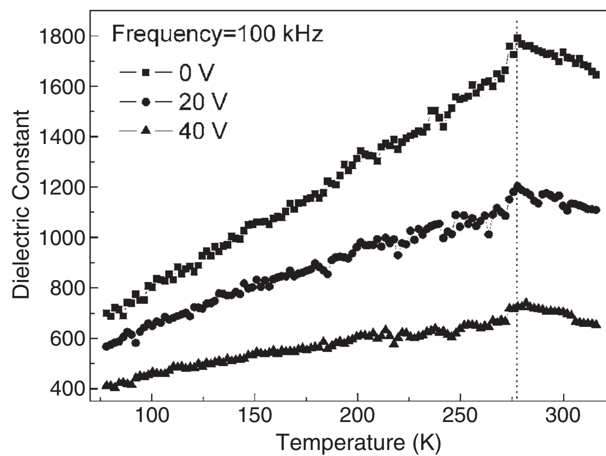

Figure 3. Temperature dependence of the dielectric constant at 100 kHz for the BST thin film, measured with no bias and 20 V and 40 V DC biases. Note that the dotted line is drawn only as a guide to the eye.

the lattice parameter of 0.379 nm) and the $Ba_{0.5}Sr_{0.5}TiO_3$ structure with the lattice constant of 0.395 nm. The orientation relationship of $[010]_{BST}//[010]_{LAO}$ and $[001]_{BST}//[001]_{LAO}$ can be obtained from the figure. Moreover, a lattice mismatch of $\sim$4.2% between $Ba_{0.5}Sr_{0.5}TiO_3$ and $LaAlO_3$ can be obtained from splits of the diffraction spots, which is in excellent agreement with the above-mentioned XRD results. The interfacial microstructure characteristics indicate the good quality of epitaxial growth and the sharp interface between the film and the substrate.

Figure 3 shows the temperature dependence of the relative dielectric constant at the frequency of 100 kHz for the BST thin film, measured with no bias and 20 and 40 V DC biases, respectively. The dotted line in the figure is drawn only as a guide to the eye. As can be seen in the three curves, the temperatures of the dielectric permittivity maximum (T_m) all occurred at around 275 K, much lower than 300 K. According to Vendik and Zubko's research [16], for a real ferroelectric material, T_m is displaced to a higher value with respect to

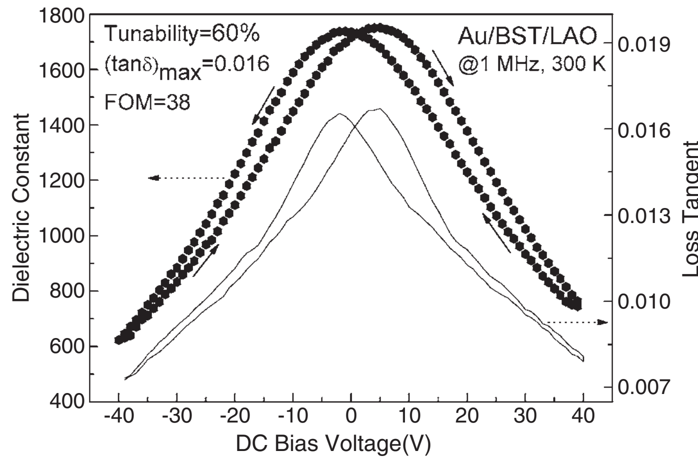

Figure 4. Applied DC bias voltage dependence of the dielectric constant and loss tangent for the BST thin film, measured at 1 MHz and 300 K.

the temperature of the true phase transition (T_c). Hence, it could be concluded that the BST thin film investigated here is in the paraelectric state at room temperature, which has been confirmed by the electron holography measurements at different temperatures [13]. It should be pointed out that a very good dielectric tunability could be acquired in the BST film at room temperature just by applying a moderate bias voltage.

Figure 4 shows the DC bias voltage dependence of the dielectric constant and loss tangent ($\tan\delta$) for the BST thin film, measured at 1 MHz and 300 K. The figure of merit (FOM), which is defined as tunability/$(\tan\delta)_{max}$, is commonly used to evaluate the overall dielectric performance of the materials for tunable microwave devices [5]. A tunability as high as 60% is obtained by applying a 40 V DC bias. Besides this, the loss tangent is relatively low with the maximum value of 0.016. Accordingly, the FOM factor reaches 38 at an electric field intensity of 40 kV cm^{-1}. The good results obtained in the dielectric property measurements demonstrate potential applications of the films in real devices. Nonetheless, the butterfly-shaped curve is obvious in both the ε_r–V and the $\tan\delta$–V relationships. This is a typical phenomenon for a ferroelectric crystal, namely, a hysteresis effect. As mentioned above, such a hysteresis effect should be avoided in the BST thin films for tunable microwave device applications. Unfortunately, similar results are also reported commonly by others [5–12]. In the following context, full effort will be devoted to elucidating the origin of this unfavourable C–V hysteresis in the paraelectric BST thin films.

Figure 5 shows the temperature dependence of the dielectric constant at zero bias, measured at various frequencies from 50 kHz to 1 MHz. The dotted line is drawn as a guide to the eye. The inset shows the corresponding loss tangent as a function of the temperature. It is markedly demonstrated that the dielectric permittivity peaks occur at various frequencies and shift to higher temperatures with increase in the frequency. Correspondingly, the dielectric loss peaks, well correlated with the permittivity peaks, are observed. It is suggested that the variation of the peak temperature (T_p) with frequency exhibits a thermally activated relaxation behaviour, and could be analysed using the Arrhenius law [17]. Here, the law can be represented as $f = f_0 \exp(-E/k_B T)$, where f_0 is the characteristic relaxation frequency at infinite temperature, E is the activation energy for the relaxation, k_B is Boltzmann's constant and T is the absolute temperature. The relaxation frequency as a function of the inverse peak

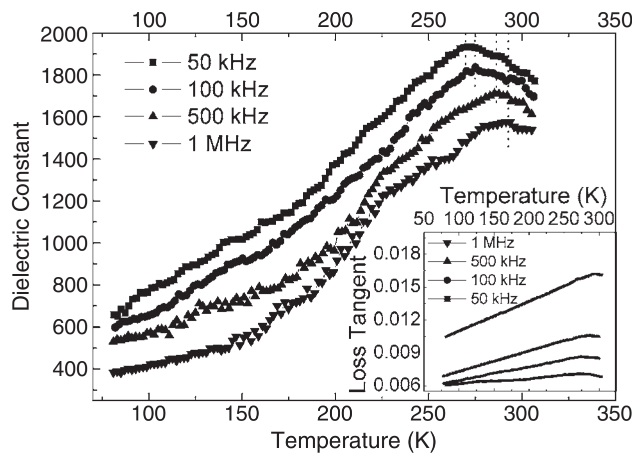

Figure 5. Temperature dependence of the dielectric constant at zero bias, measured at various frequencies from 50 kHz to 1 MHz. The dotted line is drawn as a guide to the eye. The inset shows the corresponding loss tangent as a function of the temperature.

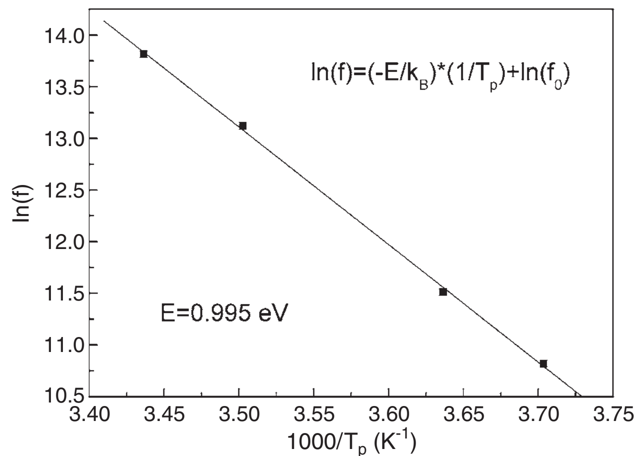

Figure 6. Arrhenius plot of the relaxation frequency with the inverse peak temperature, obtained from the dielectric loss peaks. The solid line is the linear fitting.

temperature ($1/T_p$) is plotted in the figure 6. A fairly linear relationship is obtained, indicating that the data are well fitted to the Arrhenius law. The activation energy E of 0.995 eV is obtained, which is consistent with the 1.02 eV obtained for PLD-derived multilayered thin films of $(Ba_{0.80}Sr_{0.20})(Ti_{1-x}Zr_x)O_3$ [17], where the peaks also occurred in the paraelectric phase. In accordance with their discussion, we believe that the dielectric relaxation presented here should be associated with oxygen vacancies in the BST thin film. This concept can be further confirmed from the frequency dependent dielectric constant and loss tangent characteristics, measured at different temperatures.

Figures 7(a) and (b) show the frequency dispersion curves of the dielectric constant and the loss tangent, respectively, measured at different temperatures. The dielectric constant exhibits rollover in the low frequency range at 250 K, with a loss peak (occurring at about 3 kHz) accompanying it. The loss peak shows a continuous trend of shifting towards high frequencies

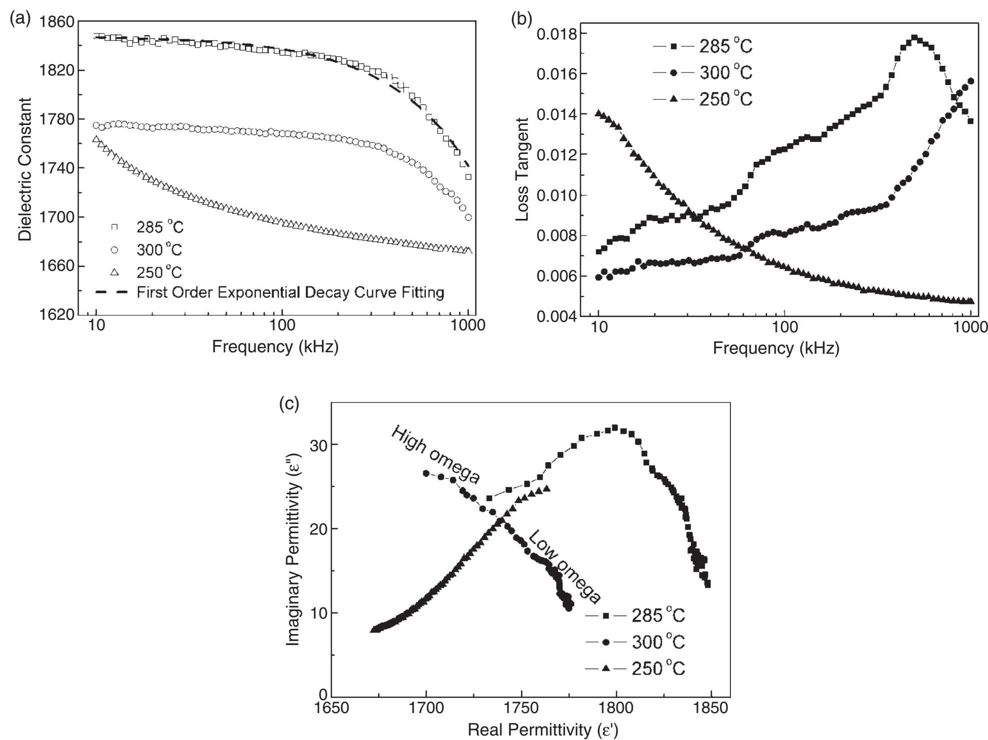

Figure 7. (a) Dielectric constant as a function of the frequency at different temperatures. The dashed line is the first-order exponential decay curve fitting. (b) Loss tangent as a function of the frequency at different temperatures. (c) Cole–Cole plots of the dispersion curves obtained at several temperatures.

at high temperatures; at temperatures up to 300 K or higher, the loss peak is out of the measured frequency window. The frequency and temperature dependent loss peaks are well coupled with the above results in figures 5 and 6. Note that the measurement data for the dielectric loss fluctuate severely at frequencies below 10 kHz; thus they are not shown here. The frequency dispersion in our sample can be confirmed to have a non-Debye-type character of the overall relaxation. In Debye-type relaxation, the loss factor should start from a zero value at zero frequency, and then should show a proportional relationship with the frequency according to $\tan\delta = \omega CR$. More evidently, the plot of imaginary permittivity (ε'') versus real permittivity (ε'), namely, the Cole–Cole plot, should lead to a semicircle for a Debye relaxation [18, 19]. In the case of our sample, however, the Cole–Cole plots for different temperature measurements show a clear divergence, as shown in figure 7(c). Note that the imaginary permittivity was calculated from $\tan\delta = \varepsilon''/\varepsilon'$. On the other hand, these results are in good agreement with a Maxwell–Wagner type of dielectric relaxation in laser ablated polycrystalline $ZrTiO_4$ thin films obtained by Victor *et al* [20]. Moreover, the frequency dispersion indicates an exponential decay of the dielectric constant, as shown in figure 7(a). This was similarly reported by Fadnavis *et al* for Nd^{3+} doped ferroelectric lead germanate single crystals, where the dielectric relaxation of Maxwell–Wagner type was observed [21]. Maxwell–Wagner relaxation and degradation were also observed in $SrTiO_3$ and $BaTiO_3$ ceramics [22]. In particular, indications of a non-Debye dielectric relaxation were found in the $Ba_{0.5}Sr_{0.5}TiO_3$ thin films grown on MgO substrates [8]. Likewise, Maxwell–Wagner-type interfacial polarization was reported in

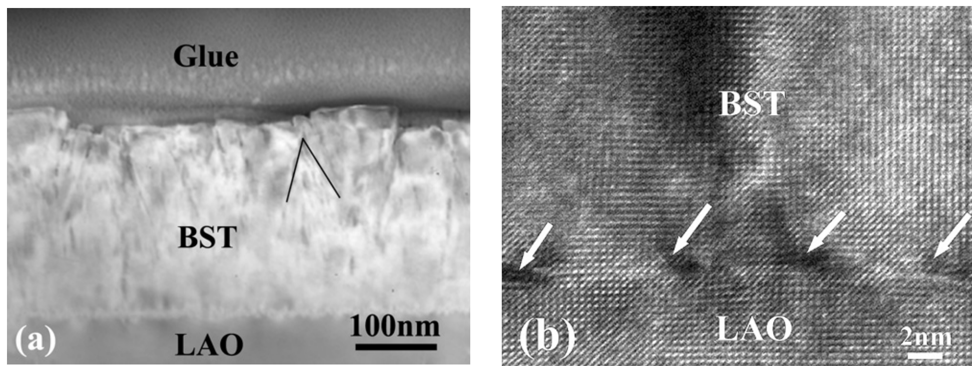

Figure 8. (a) Low magnification bright field TEM image, displaying the morphology of the BST thin film epitaxially grown on LAO. (b) HRTEM image, displaying the misfit dislocations at the film/substrate interface. Note that a filtering was performed to show the misfit dislocations more clearly.

the $Ba_{0.6}Sr_{0.4}TiO_3$ thin films prepared on $Pt/Ti/SiO_2/Si$ substrates [7]. As is well known, the Maxwell–Wagner relaxation and polarization arise from a charge accumulation at the interface between the sample and contacts or at grain boundaries [7, 20, 23]. Consequently, the above-mentioned weak hysteresis effect, indicated by the butterfly-shaped ε_r–V curve, is thought of as associated with oxygen vacancies and other space charges at the interface between the film and the substrate and/or at the grain boundaries. Oxygen vacancies, the most common point defects in titanates [24, 25], and other space charges such as the negatively charged oxygen [7] lead to the appearance of local regions of ferroelectric polarization. Tenne *et al* have provided powerful evidence for the existence of polar nanoregions by Raman study [9].

In order to give direct evidence for our discussion, we performed cross-sectional TEM and electron holography measurements. Figures 8(a) and (b) show a bright field TEM image at low magnification and a high resolution TEM image, respectively. As can be seen in figure 8(a), a clear feature of the as-grown film is the columnar structure with V-shaped grain boundaries as indicated with the solid lines. This structural feature of BST thin films is often reported by others [26–28], and it is detrimental to the electrical properties of thin films. The columnar-like growth is considered to originate at the various domains that were grown at different surface terraces on the substrate [26], and/or to result from small relative rotations between the grains [28]. Furthermore, as indicated by solid arrows in figure 8(b), there exist numerous misfit dislocations at the film/substrate interface, which were introduced to relieve the lattice mismatch strain. This dislocation array is estimated to exhibit a pseudo-periodicity of about $L = 7.5$ nm. The defects described here, namely, the grain boundaries and the interfacial misfit dislocations, are considered to be the source for the aforementioned C–V hysteresis.

Figures 9(a) and (b) show the electron holography results, measured at room temperature. Figure 9(a) shows a hologram taken from an interfacial area with clear misfit dislocations, as indicated with arrows, obtained by applying a positive bias of 120 V to the biprism. In order to clearly elucidate the misfit dislocation, a schematic drawing of the atomic arrangement is shown in the inset of figure 9(a). As expected for a paraelectric state, there is no detectable phase change at the interface position, whereas a line scan across the misfit dislocation shows remarkable phase alternations. To ameliorate the poor statistics of a single line scan, we have taken the averaged phase profile over 50 line scans in our analysis. Figure 9(b) shows the differentiation of the phase profile and could be used to predict the charge distribution around

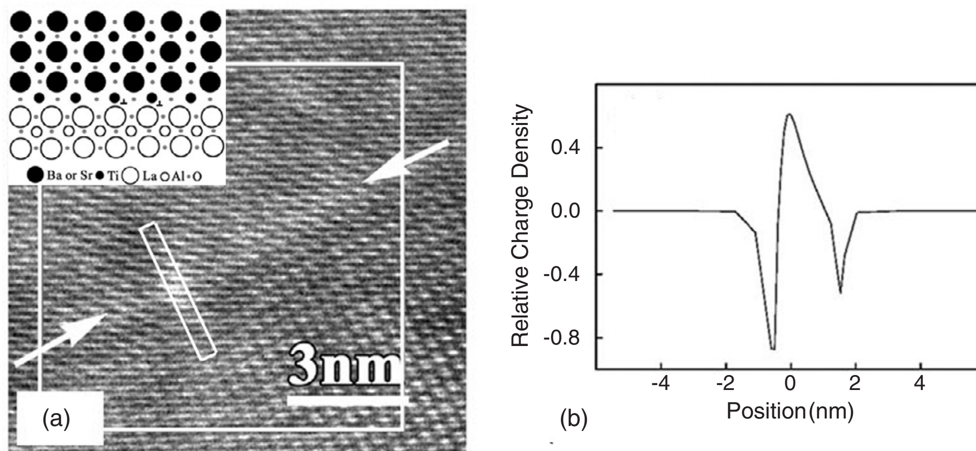

Figure 9. (a) Electron hologram taken at room temperature from an interface area with a distinct misfit dislocation, as indicated with the two arrows. The inset shows a schematic illustration of the atomic arrangement to clearly elucidate the misfit dislocation. (b) Charge distributions across the dislocation. The lines along which the charge density was measured are drawn as a slim rectangle, as displayed in figure 9(a).

the dislocation, which demonstrates positive charges accumulating on the dislocation core with negative charges around. In addition, a small amount of charges were observed to accumulate at the intragrain boundaries in our room temperature measurements. More detailed discussion of the electron holography observations can be referred to in our previous publication elsewhere [13]. To sum up, cross-sectional TEM and electron holography observations have provided us with effective evidence for space charges at the film/substrate interface and at the grain boundaries.

4. Conclusions

Highly epitaxial $Ba_{0.5}Sr_{0.5}TiO_3$ thin films with the thickness of about 350 nm have been grown on (001) $LaAlO_3$ single-crystal substrates by pulsed-laser deposition. The good crystallinity and orientation relationships are confirmed by XRD and cross-sectional TEM measurements. The as-grown BST thin films are experimentally demonstrated in the paraelectric state at room temperature. The good dielectric properties, such as a high tunability of about 60% on applying an electric field of 40 kV cm^{-1}, a relatively low loss maximum of 0.016 and, thus, a FOM factor of 38 at 1 MHz and 300 K have been successfully obtained. However, the DC bias dependence of the dielectric constant shows obviously a butterfly-shaped feature, typical for a ferroelectric material. Careful frequency and temperature dependent dielectric property measurements indicate a distinct dielectric relaxation, probably of the Maxwell–Wagner type. The dielectric relaxation could lead to drastic dielectric degradation, such as a rather high loss tangent due to the additional relaxation loss. Furthermore, the weak C–V hysteresis effect investigated in this work could be explained in terms of the Maxwell–Wagner-type dielectric relaxation, which is associated with oxygen vacancies and other space charges at the interface between the film and the substrate and/or at the grain boundaries. The cross-sectional TEM and electron holography observations give direct evidential support for our analysis and discussion. There are still a great number of defects, such as V-shaped grain boundaries and misfit dislocations, in the as-grown thin films. A small amount of space charges are confirmed to exist at the interfacial misfit

dislocations and at the grain boundaries. Further work is under way to improve the quality and related properties of BST thin films for practical applications in tunable microwave devices.

Acknowledgments

This work was financially supported by the National Natural Science Foundation of China (Grant Nos 59832050 and 10174093), the Ministry of Science and Technology of China and the Chinese Academy of Sciences.

References

[1] Chen C L, Feng H H, Zhang Z, Brazdeikis A, Huang Z J, Chu W K and Chu C W 1999 *Appl. Phys. Lett.* **75** 412
[2] Carlson C M, Rivkin T V, Parilla P A, Perkins J D, Ginley D S, Kozyrev A B, Oshadchy V N and Pavlov A S 2000 *Appl. Phys. Lett.* **76** 1920
[3] Cole M W, Hubbard C, Ngo E, Ervin M, Wood M and Geyer R G 2002 *J. Appl. Phys.* **92** 475
[4] Tagantsev A K, Sherman V O, Astafiev K F, Venkatesh J and Setter N 2003 *J. Electroceram.* **11** 5
[5] Li H C, Si W D, West A D and Xi X X 1998 *Appl. Phys. Lett.* **73** 190
[6] Hyun S and Char K 2001 *Appl. Phys. Lett.* **79** 254
[7] Pontes F M, Leite E R, Longo E, Varela J A, Araujo E B and Eiras J A 2000 *Appl. Phys. Lett.* **76** 2433
[8] Hubert C, Levy J, Cukauskas E J and Kirchoefer S W 2000 *Phys. Rev. Lett.* **85** 1998
[9] Tenne D A, Soukiassian A, Zhu M H, Clark A M, Xi X X, Choosuwan H, He Q, Guo R and Bhalla A S 2003 *Phys. Rev.* B **67** 012302
[10] Xia Y D, Cheng J B, Pan B, Wu D, Meng X K and Liu Z G 2005 *Appl. Phys. Lett.* **87** 052902
[11] Booth J C, Takeuchi I and Chang K S 2005 *Appl. Phys. Lett.* **87** 082908
[12] Zhai J W, Yao X, Zhang L Y and Shen B 2004 *Appl. Phys. Lett.* **84** 3136
[13] Tian H F, Yu H C, Zhu X H, Wang Y G, Zheng D N, Yang H X and Li J Q 2005 *Phys. Rev.* B **71** 115419
[14] Gevorgian S, Carlsson E, Rudner S, Wernlund L D, Wang X and Helmersson U 1996 *IEE Proc.* H **143** 397
[15] Gevorgian S S, Martinsson T, Linner P L J and Kollberg E L 1996 *IEEE Trans. Microw. Theory Tech.* **44** 896
[16] Vendik O G and Zubko S P 2000 *J. Appl. Phys.* **88** 5343
[17] Cheng B L, Wang C, Wang S Y, Button T W, Lu H B, Zhou Y L, Chen Z H and Yang G Z 2004 *Appl. Phys. Lett.* **84** 5431
[18] Wei Y Z and Sridhar S 1993 *J. Chem. Phys.* **99** 3119
[19] Yusoff A R M and Abd Majid W H 2005 *Eur. Phys. J.* B **45** 33
[20] Victor P, Bhattacharyya S and Krupanidhi S B 2003 *J. Appl. Phys.* **94** 5135
[21] Fadnavis S A and Katpatal A G 1997 *Ferroelectrics* **200** 81
[22] Neumann H and Arlt G 1986 *Ferroelectrics* **69** 179
[23] Lunkenheimer P, Bobnar V, Pronin A V, Ritus A I, Volkov A A and Loidl A 2002 *Phys. Rev.* B **66** 052105
[24] Waser R and Smyth D M 1996 *Ferroelectric Thin Films: Synthesis and Basic Properties* ed C P de Araujo, J F Scott and G W Taylor (Amsterdam: Gordon and Breach) p 47
[25] Scott J F 2000 *Ferroelectric Memories* (Berlin: Springer) pp 140–3
[26] Chen C L, Shen J, Chen S Y, Luo G P, Chu C W, Miranda F A, Van Keuls F W, Jiang J C, Meletis E I and Chang H Y 2001 *Appl. Phys. Lett.* **78** 652
[27] Baumert B A, Chang L H, Matsuda A T, Tsai T L, Tracy C J, Gregory R B, Fejes P L, Cave N G, Chen W, Taylor D J, Otsuki T, Fujii E, Hayashi S and Suu K 1997 *J. Appl. Phys.* **82** 2558
[28] Gao H J, Chen C L, Rafferty B, Pennycook S J, Luo G P and Chu C W 1999 *Appl. Phys. Lett.* **75** 2542

INSTITUTE OF PHYSICS PUBLISHING JOURNAL OF PHYSICS: CONDENSED MATTER
J. Phys.: Condens. Matter **18** (2006) 10117 doi:10.1088/0953-8984/18/40/C02

Erratum

The origin of the weak ferroelectric-like hysteresis effect in paraelectric $Ba_{0.5}Sr_{0.5}TiO_3$ thin films grown epitaxially on $LaAlO_3$
X H Zhu 2006 *J. Phys.: Condens. Matter* **18** 4709–4718

The unit °C in figures 7(a), 7(b) and 7(c) should be K.